J. Integr. Sci. Technol. 2025, 13(4), 1071

Journal of Integrated
SCIENCE& TECHNOLOGY

Exploring the dielectric characteristics of NBT-MFO multiferroic nanocomposites for enhanced energy storage applications

Monika Dhall,[1] Satish Khasa,[*1] Ashima Hooda,[1] Jyoti Shah,[2] R.K. Kotnala[2]

[1]Material Research Laboratory, Department of Physics, Deenbandhu Chhotu Ram University of Science & Technology, Murthal – 131039 (Sonipat), Haryana, India. [2]CSIR-National Physical Laboratory, New Delhi, 110012, India.

Submitted on: 28-Oct-2024, Accepted and Published on: 10-Jan-2025

Article

ABSTRACT

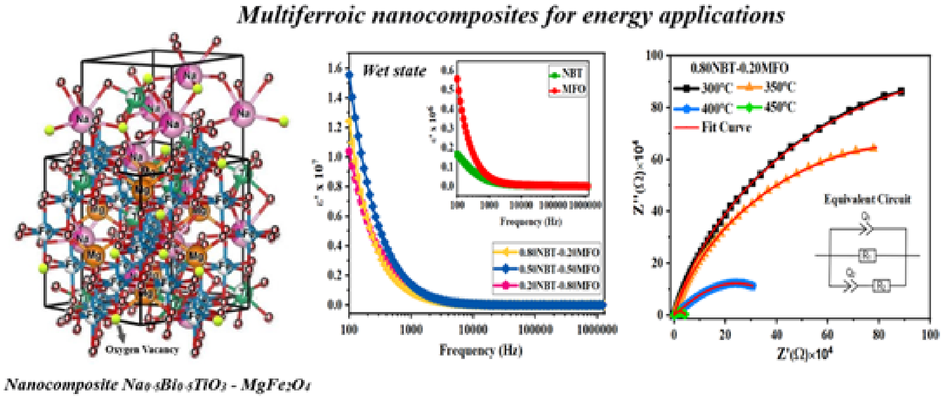

Multiferroic nanocomposites with the composition (1-x) $Na_{0.5}Bi_{0.5}TiO_3$ - (x) $MgFe_2O_4$, for x values of 0, 0.2, 0.5, 0.8, and 1.0, have been synthesized using the established solid-state reaction technique. A comprehensive dielectric analysis revealed significant enhancements in the dielectric properties of the nanocomposites compared to their single-phase counterparts. The relative permittivity (ε') and dielectric loss (ε''), both revealed behavior indicative of Maxwell-Wagner polarization, with pronounced dispersion observed at lower frequencies and higher temperatures. The multiferroic 0.50NBT-0.50MFO and 0.80NBT-0.20MFO nanocomposites displayed the highest dielectric constant, attributed to significant cationic disorder within the structure. The frequency-dependent capacitance and dielectric constant in the wet state revealed the promising potential of these nanocomposites for hydroelectric cell applications, due to increased lattice defects, porosity, oxygen vacancies, and unsaturated surface cations compared to single-phase NBT and MFO. The overlapping normalized impedance and modulus curve, converging onto a unified master curve, indicated temperature-invariant dynamic processes governing conduction and spatially confined relaxation. The Nyquist curves of impedance presented semicircular arcs that were suppressed, indicative of non-Debye relaxation, while the decrease in arc radii with rising temperature highlighted the semiconducting nature of the synthesized system. These findings underscore the potential of these nanocomposites for advanced applications in electronics and energy storage systems.

Keywords: Nanocomposites, Dielectric permittivity, Electric Modulus, Nyquist plot, Energy applications

INTRODUCTION

Materials scientists and engineers dedicated to developing novel materials constantly seek to establish a clear connection between a material's structure and its properties, aiming to optimize these properties for specific device applications. One notable class of such materials, multiferroics or "smart materials," has gained significant attention in research due to their unique fundamental physics and versatile applications. These materials, which exhibit two or more coupled ferroic properties, can have their characteristics substantially modified by external factors such as electric and magnetic fields. Their promising applications in spintronics, memory storage, sensing devices and energy harvesting etc. make them a hot area of research[1]. As research progresses to enhance the performance of these materials and address current limitations, multiferroics are set to play a crucial function in developing future electronic devices and technologies. In practical terms, multiferroic properties manifest either in single-phase materials where magnetic and electric polarization coexist simultaneously, or within composite structures comprising two distinct phases. However, the realization of electric polarization induced by magnetization, known as the magnetoelectric (ME) effect, and conversely, is often difficult to attain in single-phase multiferroics. As a result, these materials

---

*Corresponding Author: Prof. Satish Khasa, Department of Physics, Deenbandhu Chhotu Ram University of Science & Technology, Murthal, 131039, India
Tel: +919812818900; Email: skhasa.phy@dcrustm.org

Cite as: *J. Integr. Sci. Technol., 2025, 13(4), 1071.*
URN:NBN:sciencein.jist.2025.v13.1071
DOI:10.62110/sciencein.jist.2025.v13.1071

offer limited technological advantages, primarily due to the rigorous temperature limitations that constrain their effectiveness.[2]

Multiphase composites have demonstrated remarkable ME effects, even at ambient temperature.[3] Van Suchetelene[2] initially proposed that the magnetoelectric response in composite materials arise from the interplay of their combined properties. Consequently, ferrite-ferroelectric composites are considered the most promising solution for enhancing electrical, magnetic properties and overcoming the limitations of monophase ME materials, such as high leakage currents, limited magnetoelectric coefficients, and suboptimal performance at low temperatures.[3] While various lead-based ME materials have shown significant effects, the toxicity of lead has spurred research into Lead-free ferrite-ferroelectric materials that produce equivalent outcomes. Sodium Bismuth Titanate, $Na_{0.5}Bi_{0.5}TiO_3$ (NBT) has been demonstrated to be an effective substitute for PZT, exhibiting comparable piezoelectric, ferroelectric, and electrical properties.[4] The relaxor ferroelectric behavior of NBT is ascribed to the chaotic arrangement of cations and the non-polar nature of its atomic structure, coupled with the tilting of its octahedra. Additionally, NBT is recognized as a primary material for producing lead-exempt composites, as highlighted by S.N. Babu et al.[5]

Ferrites are a group of ceramic materials primarily composed of iron oxide (Fe_2O_3) combined with various metal oxides, such as magnesium, manganese, zinc, nickel, or cobalt. These compounds are indispensable in numerous technological and industrial sectors due to their distinctive magnetic, electrical, and mechanical properties. Ferrites are particularly prevalent in high-frequency electronics, electromagnetic devices, and energy systems.[6] Among them, magnesium ferrite ($MgFe_2O_4$) stands out as a type of spinel ferrite, known for its notable magnetic and electrical characteristics. As a soft ferrite, magnesium ferrite exhibits low coercivity, allowing it to be easily magnetized and demagnetized, while its high resistivity makes it especially suitable for high-frequency applications.[7] Multiferroic composites can display improved or adjustable dielectric properties when various ferroic phases are combined. Analyzing their dielectric behavior aids in fine-tuning these properties for targeted applications, including high-frequency electronics, signal processing, energy storage devices, tunable capacitors, and microwave components.

A variety of NBT based ferrite composites have recently been explored, such as... (NBT-$NiFe_2O_4$),[8] (NBT-$BaFe_{12}O_{19}$),[3] (NBT-$MnFe_2O_4$).[6] S. Dagar et al. have studied the structural, improved dielectric and magnetic characteristics of (NBT-$Ni_{0.25}Mg_{0.5}Zn_{0.25}Fe_2O_4$)[9] and (NBT-$Ni_{0.25}Co_{0.5}Zn_{0.25}Fe_2O_4$)[4] composite systems, revealing improved dielectric constants for composites than the individual pure ones. In light of this, principal aim of this investigation is to examine the dielectric properties of $Na_{0.5}Bi_{0.5}TiO_3$ - $MgFe_2O_4$ multiferroic nanocomposites for potential energy storage applications. Recent research have highlighted the use of $Na_{0.5}Bi_{0.5}TiO_3$-$MgFe_2O_4$ magnetoelectric nanocomposites for environmentally sustainable power generation through Hydroelectric cells (HECs).[10] However, to date, there has been no experimental investigation into the dielectric characteristics of these nanocomposites. Consequently, the current research is dedicated to exploring the optimized dielectric and impedance characteristics of $Na_{0.5}Bi_{0.5}TiO_3$ - $MgFe_2O_4$ nanocomposites within the context of energy-related applications.

EXPERIMENTAL

Materials and Methods

The mutliferroic nanocomposites, characterized by the chemical composition (1-x) $Na_{0.5}Bi_{0.5}TiO_3$ - (x) $MgFe_2O_4$ were fabricated using the solid-state reaction technique. The compositions examined include $x = 0$ (NBT), $x = 0.2$ (0.80NBT-0.20MFO), $x = 0.5$ (0.50NBT-0.50MFO), $x = 0.8$ (0.20NBT-0.80MFO) and $x = 1$ (MFO). Analytical grade oxide precursors were employed in the synthesis. The detailed synthesis process has been discussed in previous literature[10]. The final products were achieved by sintering the calcined pure and composite powders at 850°C for 2 hours. Pellets, with a thickness of approximately 0.1 cm and a radius of 0.5 cm, were fabricated using these samples prior to the sintering process.To ensure optimal electrode connections, the pellets were coated with silver paint on both sides. The crystal structure, purity and phase identification study of the developed samples have been established through X-ray diffraction (XRD) with a Rigaku Ultima IV diffractometer employing Cu Kα radiation, across a 2θ range of 20° to 80°, at a scan speed of 2°/min.. In the current study, the samples were characterized through dielectric, modulus, and impedance analyses. Dielectric properties were assessed with a Hioki 3532-50 LCR Hi-Tester, spanning a temperature range from ambient temperature (RT) to 400°C, and frequency range from 100 Hz to 5 MHz.

RESULT AND DISCUSSIONS

Dielectric Study

The study of dielectrics is a fundamental aspect of electrical physics. A dielectric material is characterized by being a poor conductor of electricity and having the ability to be polarized by an electric field. Upon the application of an electric field, the molecules within the material undergo a displacement, resulting in an induced dipole moment. This polarization enables the material to store electrical energy. To comprehend a dielectric's behavior under different conditions, it's essential to examine its permittivity which indicates how easily the material can be polarized. Relative permittivity (or dielectric constant) measures this ability in comparison to a vacuum.

In practical applications, particularly at high frequencies, materials show, not only energy storage but also energy loss due to factors such as conductivity and dielectric relaxation. This is where complex permittivity is important. It consists of two components: the real part, which signifies the energy preserved, and the imaginary component, which indicates the energy dissipated.[11]

Complex permittivity provides a more complete understanding of a dielectric's behavior, particularly in AC fields and high-frequency scenarios, which is expressed by the equation below:

$$\varepsilon^* = \varepsilon' + \varepsilon'' \tag{1}$$

$$tan\delta = (\varepsilon''/\varepsilon') \tag{2}$$

The real component (ε′) corresponds to the material's relative permittivity or dielectric constant, whereas the imaginary component (ε′′) is linked to its dielectric loss. Dielectric loss is mainly attributed to the material's delayed reaction to the applied electric field. Dielectric loss tangent (tanδ) arises as the electric field intensifies, resulting in the polarization trailing behind the field[9].

Figure 1 shows how the dielectric constant (ε′) and loss tangent (tanδ, displayed in the inset) change with frequency across all the samples at different temperatures. In ceramics, dielectric properties arise from both intrinsic and extrinsic factors. Intrinsic factors are related to the material's structural characteristics, while extrinsic factors involve physical and chemical elements like dopants, defects, and microstructures. Both the dielectric constant and tanδ exhibit dispersive behavior at lower frequencies, becoming nearly constant at higher frequencies, which is a typical characteristic of dielectric materials. This behavior aligns well with the Maxwell-Wagner model and Koop’s theory.[9,12]

The Maxwell-Wagner theory describes the behavior of heterogeneous dielectric materials, particularly in relation to their electrical properties and the mechanisms behind polarization. The theory explains how polarization occurs due to the displacement of charge carriers. This can involve ionic or dipolar contributions, which can vary based on frequency and temperature. At lower frequencies, all polarization mechanisms collectively influence the dielectric constant. As frequency increases, these contributions diminish sequentially, leading to a scenario where, at higher frequencies, only the electronic polarization significantly affects the dielectric constant.[13] In heterogeneous dielectrics, there are interfaces that can lead to charge accumulation. This interfacial polarization significantly affects the overall dielectric dispersion response at lower frequencies. The dielectric properties of materials often change with frequency. The Maxwell-Wagner effect illustrates how lower frequencies allow more time for charge carriers to respond, enhancing polarization effects. At higher frequencies, this response diminishes.[14]

As per the Koop’s phenomena, a dielectric substance can be conceptualized as comprising strongly conductive regions i.e. grains linked by grain boundaries that are less conductive. At high frequencies, grains have a more prominent influence on ε′ i.e. dielectric constant, whereas at low frequencies, grain boundaries exert a more substantial effect. When an external field is applied, polarization predominantly takes place at the grain boundaries, driven by the existence of charge carriers and conductive pathways. At low frequencies, charge carriers gather at the junctions between grains, as the grain boundaries exhibit high resistance, leading to increased polarization. Consequently, the dielectric permittivity is elevated in the reduced frequency range.[4,15] Cationic disorder plays a vital part in shaping the dielectric properties of materials, with the dielectric constant increasing as cationic disorder rises[12]. Notably, the highest dielectric constant is recorded for 0.50NBT-0.50MFO and for 0.80NBT-0.20MFO, as these demonstrated the greatest degree of disorder among all the compositions studied, as elucidated by the XPS and Photoluminescence spectra.[10] Dielectric materials with high dielectric constants at low frequencies and elevated temperatures are vital for energy storage systems, power conversion devices, and renewable energy applications, where stability and efficiency under demanding conditions are critical for optimal performance.

Loss Tangent

The loss tangent, or tan δ, quantifies the energy dissipation in dielectric materials when exposed to an alternating electric field. It represents the ratio of dielectric loss to dielectric storage, providing insight into the efficiency of a material in applications where minimizing energy loss is crucial. Understanding the loss tangent is essential for optimizing the performance of capacitors and insulation in various high-frequency and high-temperature environments. The loss tangent behaves similar to dielectric constant and is consistent with Koop's theory. The high tanδ values observed at lower frequencies are attributed to space charge polarization. Factors that commonly lead to space charge polarization in materials include inhomogeneities in the dielectric structure, such as impurities, porosity, and grain structure.The model suggests that, at lower frequencies, the high resistivity of grain boundaries makes it harder for charge carriers to overcome

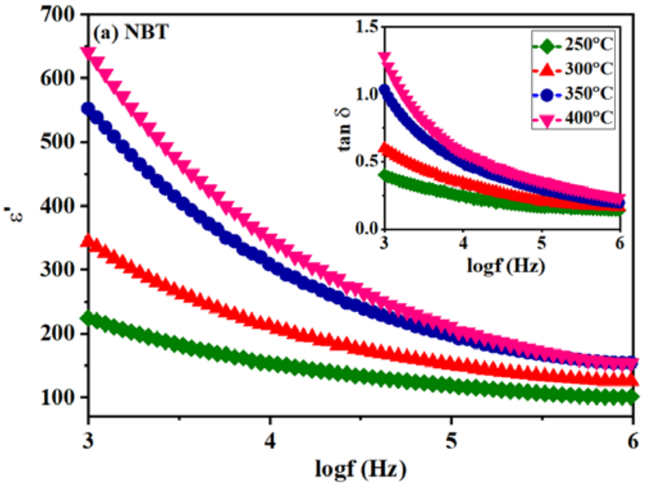

Figure 1(a). Frequency dependence of the dielectric constant (ε′) and tanδ (in inset) at various temperatures for pure NBT.

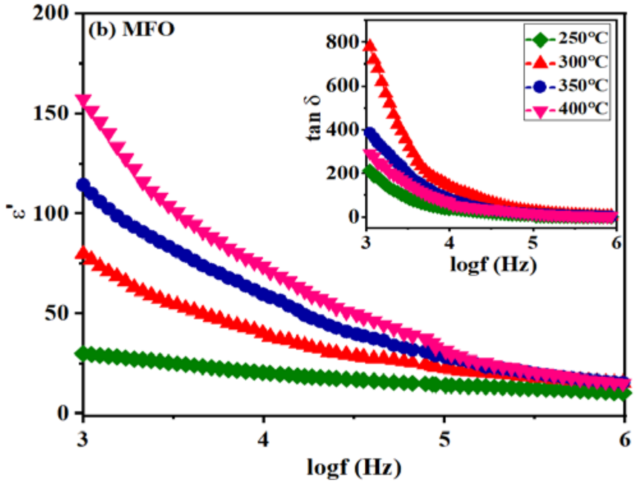

Figure 1(b). Frequency dependence of ε′ and tanδ (in inset) at various temperatures for pure MFO.

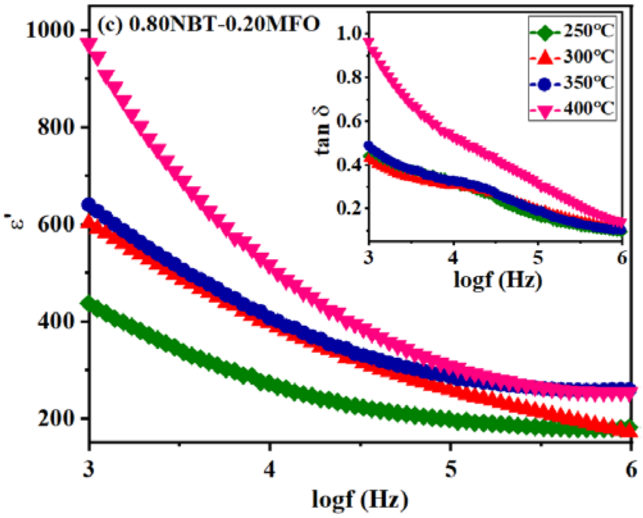

Figure 1(c). Frequency dependence of ε' and $\tan\delta$ (in inset) at various temperatures for nanocomposite 0.80NBT-0.20MFO.

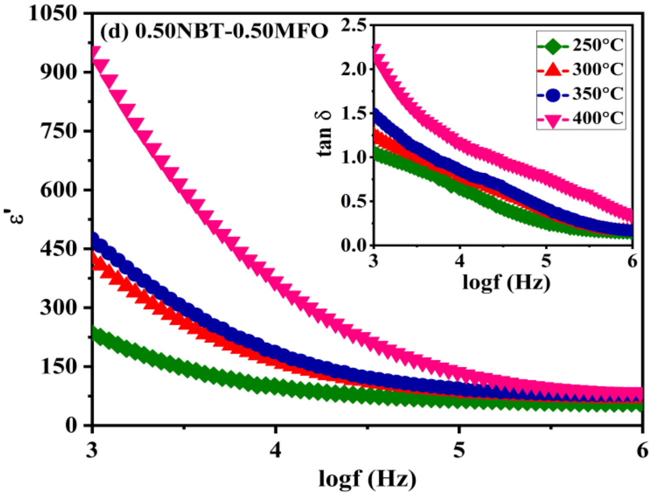

Figure 1(d). Frequency dependence of ε' and $\tan\delta$ (in inset) at various temperatures for nanocomposite 0.50NBT-0.50MFO.

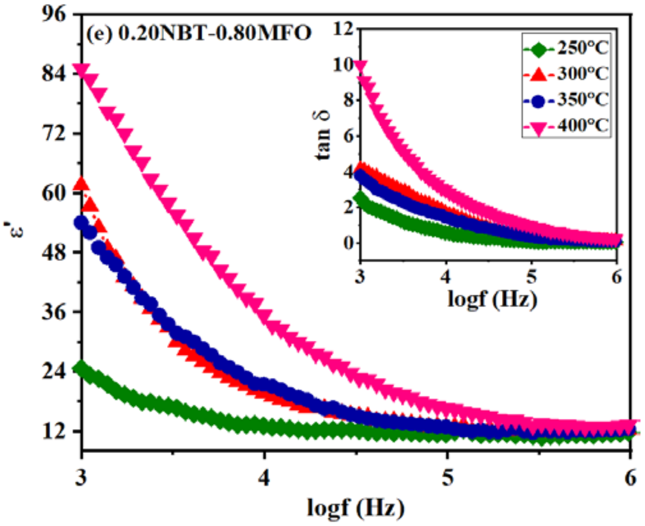

Figure 1(e). Frequency dependence of ε' and $\tan\delta$ (in inset) at various temperatures for nanocomposite 0.20NBT-0.80MFO.

obstacles, resulting in a larger $\tan\delta$. Conversely, at higher frequencies, charge carriers require less energy, leading to a decrease in $\tan\delta$.[12] In the case of composites, the tangent loss of pure ferrite MFO and nanocomposites is greater than that of NBT, attributed to the presence of magnesium, which has electrical leakage properties.[16]

Figure 2(a-e) depicts the temperature-sensitive characteristics of ε' and $\tan\delta$ across various frequencies across all synthesized samples. It is noted that as the temperature rises, both ε' and $\tan\delta$ increase until reaching the transition temperature, after which they decrease. This behavior is commonly observed in pure and composite ceramics. NBT reveals two distinct dielectric anomalies, each reflecting a diffused phase transition: The initial peak occurs at approximately 185°C, marking the temperature at which the phase changes from the ferroelectric i.e. (rhombohedral) to the antiferroelectric i.e. (rhombohedral + tetragonal) phase, commonly referred to as the depolarization temperature, T_d. The low-temperature inflection in permittivity observed within the span of (185−385)°C is believed to correspond to an intermediate state. It is suggested that the sample adopts an antiferroelectric configuration between this inflection and the Curie temperature (T_c). The second peak aligns with the Curie temperature (T_c = 385°C), which represents the transition of the phase from the ferroelectric i.e. (tetragonal) state to the paraelectric state, where both phases simultaneously exist. These results corroborate findings reported by other researchers in the field.[17,18] Pristine spinel ferrite, MFO, displays an irregularity at a reduced temperature (290°C); however, ε' begins to rise as temperature rises, suggesting the potential for another irregularity at elevated temperatures. This behavior may be linked to conduction occurring within the ferromagnetic grains and their boundaries. At reduced temperatures (beneath the transition threshold), dipoles struggle to align with the external electric field, which results in limited dielectric polarization and a reduced ε'. In contrast, at elevated temperatures, dipoles gain adequate thermal energy to align with the oscillations of the applied field, resulting in enhanced polarization and an increased ε'. The composite structure demonstrates a pair of anomalies: one at diminished temperatures (around 285-300°C) and another at higher temperatures, exceeding 400°C. In the case of the NBT dielectric, the dielectric constant exhibits an increase with rising temperature, attributable to space charge polarization and the sample's conductivity.[19] For MFO, this enhancement arises from heightened space charge polarization, driven by the increased hopping of electrons as well as hole hopping as the temperature escalates. This phenomenon leads to a reduction in the resistive properties of grain boundaries, subsequently augmenting the localized displacement of charge carriers along the axis of the electric field, which ultimately induces polarization within the dielectric.[20] For the nanocomposites (x = 0.2, 0.5, and 0.8), the observed rise in ε' till T_c can be attributed to a pair of primary factors. First, there is an amplification of space charge accumulation polarization at the boundary between the MFO and NBT phases. Second, the electron hopping among ions within the MFO phase further contributes to this effect. This electron mobility facilitates local displacement along the axis of the

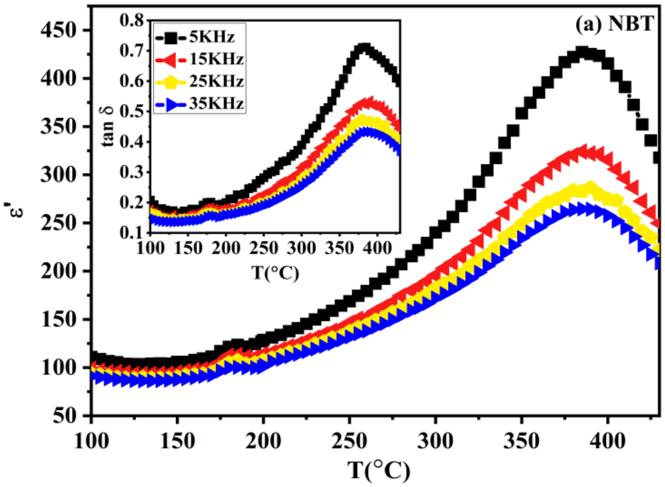

Figure 2(a). Temperature-dependent variations of ε' and $\tan\delta$ (shown in the inset) at different frequencies for single phase NBT.

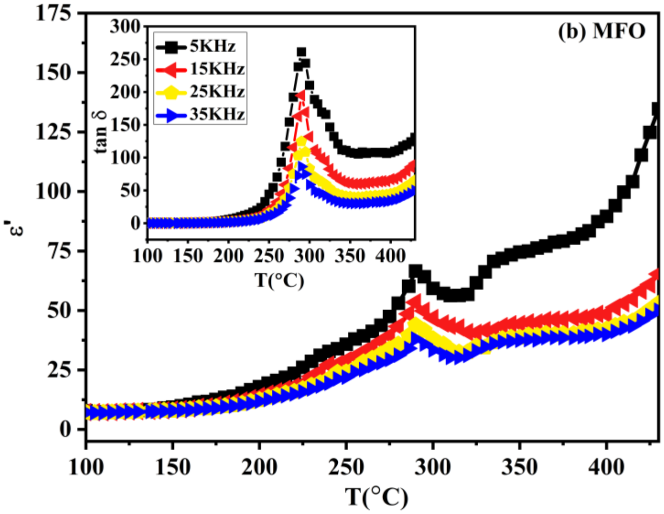

Figure 2(b). Temperature-dependent variations of ε' and $\tan\delta$ (shown in the inset) at different frequencies for single phase MFO.

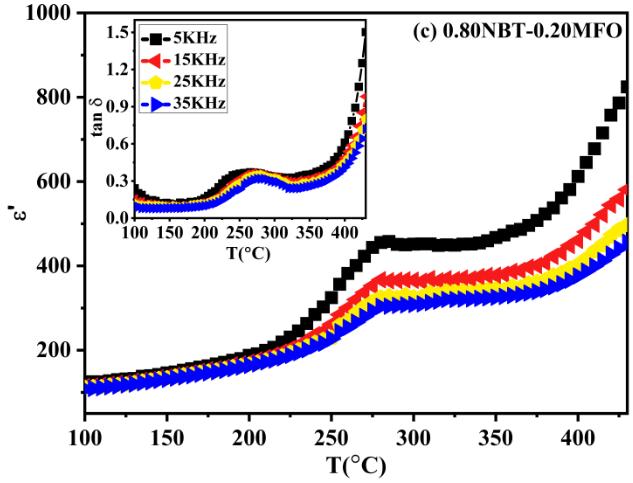

Figure 2(c). Temperature-dependent variations of ε' and $\tan\delta$ (in inset) at different frequencies for nanocomposite 0.80NBT-0.20MFO.

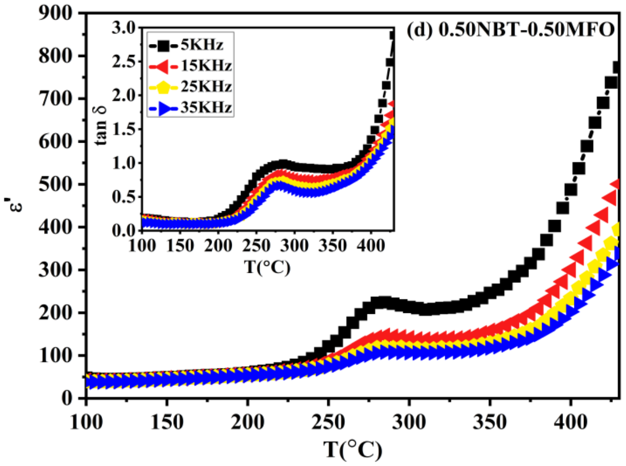

Figure 2(d). Temperature-dependent variations of ε' and $\tan\delta$ (in inset) at different frequencies for nanocomposite 0.50NBT-0.50MFO.

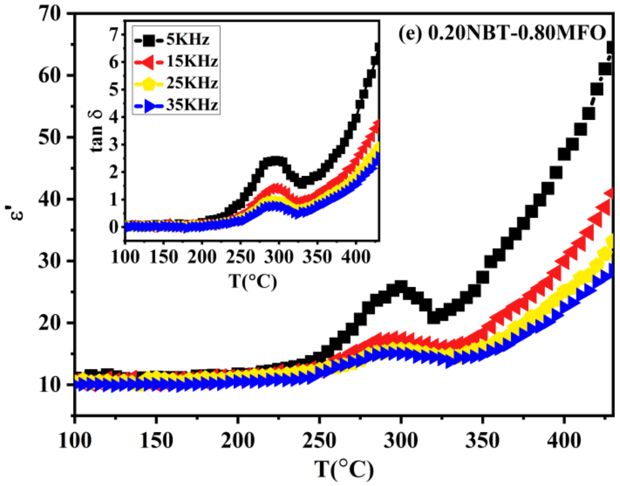

Figure 2(e). Temperature-dependent variations of ε' and $\tan\delta$ (in inset) at different frequencies for nanocomposite 0.20NBT-0.80MFO.

applied field, and since this hopping is thermally induced, it results in heightened dielectric polarization and conductivity, ultimately leading to an increase in the dielectric constant and tangent loss.[21]

The heightened values of tanδ at elevated temperatures (shown in Figure 2(a-e), in the inset) arise from an increase in charge carriers, their mobilities, and improved electrical conduction, in contrast to reduced temperatures, which are linked to conduction losses.[22] The pronounced increase at elevated temperatures correlates with the hopping rate, which accelerates with temperature. According to Koop's model, the maximum tangent loss arises when the hopping rate coincides with the frequency of the applied electric field.[15]

Figure 3(a) presents the capacitive characteristics of the synthesized sintered samples at room temperature in a wet state, recorded over a frequency spectrum of 100 Hz to 5 MHz. At lower frequencies, all the sample pellets demonstrate a high capacitance; however, this capacitance diminishes as the frequency increases. Utilizing the capacitance data, the dielectric constant of the ferrite samples has been determined using the following equation:

$$C = \varepsilon' \varepsilon_o A/d, \tag{3}$$

Here, C, ε_0, ε', A, and d denote the capacitance, vacuum permittivity, dielectric constant, surface area of pellet, and the pellet's thickness, respectively.[23]

Figures 3(b) depict the changes in dielectric constant of the produced wet samples, revealing a decline with rising frequency. At lower frequencies, the dominant polarizations namely; dipolar and interfacial, contribute to an increase in the material's dielectric permittivity. At elevated frequencies, dipolar polarization diminishes while electronic polarization intensifies, leading to a reduced dielectric constant and a stability that remains independent of frequency. These phenomena typically arise from factors such as porosity, oxygen vacancies, and grain configuration, leading to inhomogeneities within the dielectric composition[24]. The occurrence of increased lattice irregulaties, porosity, oxygen vacuities, and unsaturated surface cations in nanocomposites, in contrast to single-phase NBT and MFO, has been substantiated through prior studies[10]. The plots above clearly support the potential of these compositions for electrical energy generation via hydroelectric cell applications.

The generation of electric power in these nanocomposites-based hydroelectric cells (HECs) has been extensively investigated and analyzed, with particular focus on the strain-induced asymmetry within the perovskite phase, which induces oxygen vacancies that, in turn, alter the oxidation states of metal cations in the material. A thorough investigation was conducted, examining aspects such as structural distortion, defects, and porosity, supported by a range of characterization techniques including X-ray diffraction (XRD), Rietveld refinement, Field-emission scanning electron microscopy (FESEM), X-ray photoelectron spectroscopy (XPS), Photoluminescence (PL), voltage–current polarization, Impedance spectroscopy, and AC conductivity measurements at ambient temperature[10]. Furthermore, the presence of dissociated hydronium (H_3O^+) and hydroxide (OH^-) ions adsorbed on the surface layer of the cell pellet can be elucidated through the dielectric analysis of the fabricated (1-*x*) NBT-(*x*) MFO hydroelectric cells, where $0 \leq x \leq 1$. A notable enhancement in the capacitance values of nanocomposite-based HEC pellets has been observed in comparison to pure HEC pellets, likely attributed to the formation of local dipoles. The dissociation of ions (H_3O^+ and OH^-) at both electrodes, as well as within the lattice structure, contributes to the generation of interfacial or surface charge, further augmenting the capacitance of the nanocomposite HEC pellets. The phenomenon of dielectric dispersion within the nanocomposite HEC has resulted in the establishment of a double capacitive layer (Gupta et al. 2021a). Consequently, the observed increase in capacitance in the nanocomposite HEC pellets also corroborates a heightened degree of chemidissociation of water molecules.[25] The maximum value of capacitance and dielectric constant observed in 0.50NBT-0.50MFO further support the utmost current delivered by this nanocomposite based hydroelectric cell. Moreover, due to the substantial occurrence of oxygen vacancies, structural defects, porosity and dangling bonds on the surface, the HEC constructed with 0.50NBT-0.50MFO composition demonstrated the highest offload current.

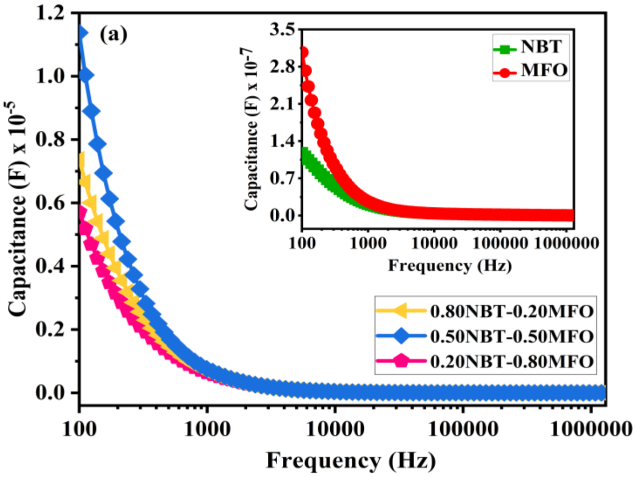

Figure 3(a). Capacitance vs. frequency plots for composites (1-x) NBT-(x) MFO, with (x = 0.2, 0.5, and 0.8), alongside pure samples (x=0 and 1) shown in the inset, measured in the wet state.v2w

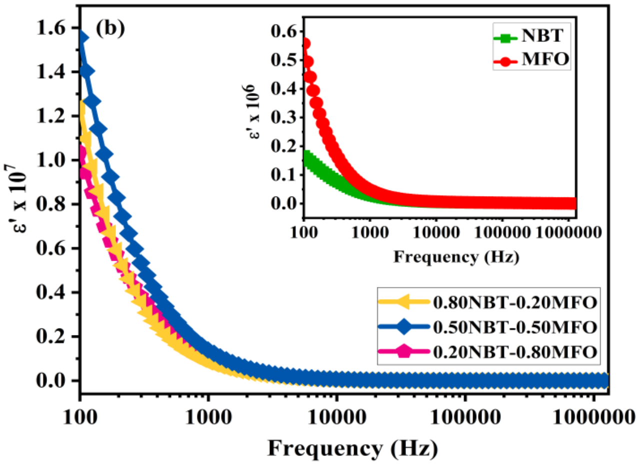

Figure 3(b). Dielectric constant vs. frequency plots for composites (1-x) NBT-(x) MFO, with (x = 0.2, 0.5, and 0.8), alongside pure samples (x= 0 and 1) shown in the inset, measured in the wet state.

Impedance Analysis

Complex Impedance Spectroscopy (CIS) is an essential method for examining the electrical characteristics and behavior of the material at multiple scales. Polycrystalline materials are composed of many individual crystallites or grains, which are separated by grain boundaries. Each of these components—grains, grain boundaries, and electrode interfaces—contributes differently to the overall electrical response of the material, and CIS allows for detailed analysis of these effects. By subjecting the material to an alternating current (AC) voltage and recording the corresponding current response, CIS offers a detailed frequency-dependent view of the material's impedance.

The complex impedance Z* is typically expressed as:

$$Z^* = Z' + jZ'' \tag{4}$$

Where Z′ is the real part of the impedance representing the resistive component (energy dissipation) and Z″ represents the imaginary component of the impedance, associated with the reactive component (energy storage or phase shift). This separation of the impedance into real and imaginary components facilitates the analysis of various mechanisms such as conduction, polarization, and relaxation processes within the material.[26] Consequently, Complex Impedance Spectroscopy is essential for enhancing the comprehension and progression of advanced materials for a wide range of applications, such as sensors, energy storage systems, and electronic components.

Figure 4(a) presents the relationship between real impedance, Z′ and frequency across a temperature span of 325 °C to 425 °C for multiferroic 0.50NBT-0.50MFO sample. It is visible that as both frequency and temperature increase, Z′ exhibits a downward trend, indicating a rise in conductivity. The observed reduction in Z′ with rising temperature points to a decrease in the resistive effects from the grains, their boundaries, and electrode junctions, which is characteristic of negative temperature coefficient of resistance (NTCR) behavior exhibited by the sample.[27] Figure 4(b) illustrates the behavior of the reactive impedance (Z″) for 0.50NBT-0.50MFO nanocomposite sample in relation to frequency at different temperatures. In the lower frequency region, the Z″ value remains stable; however, as the frequency increases, a marked rise occurs, peaking at a particular frequency known as relaxation frequency. This peak, more noticeable at lower temperatures, offers insights into the various factors influencing the electrical properties of the sample, such as the contributions from grains, grain boundaries, and the interfacial electrode effect. As temperature increases, the relaxation peak moves to higher frequency and its intensity decreases, leveling off above 375 °C. This reduction in peak intensity signals an increase in conductivity, due to the activation of charge carrier hopping at higher temperatures. The shift to higher frequencies with rising temperature reflects a decrease in relaxation time—the time it takes for induced dipoles to realign with the changing electric field. At higher temperatures, the relaxation time shortens, meaning charge carriers can't keep up with the fast-changing field leading to an increase in relaxation frequency, ultimately causing a drop in the dielectric constant at high frequencies.[28]

Figure 4(c) illustrates the normalized complex impedance (Z''/Z''_{max}) plotted against the normalized frequency $\log(f/f_{max})$, where f_m represents the resonance frequency analogous to Z''_{max}, for the 0.50NBT-0.50MFO sample at distinct temperatures. A distinct peak, known as the relaxation frequency (f_{max}), appears at a specific frequency. The sample exhibits consistent behavior across temperatures ranging from 325 °C to 425 °C, with the normalized impedance curves overlapping to form a single master curve. This overlapping confirms the subsistence of relaxation dynamics in the sample and indicates that the relaxation peak remains consistent across different temperatures.[12] All the fabricated pristine and nanocomposite samples exhibit analogous behavior in their impedance versus frequency characteristics, as exemplified by multiferroic 0.50NBT-0.50MFO sample in Figure 4(a) to Figure 4(c).[12]

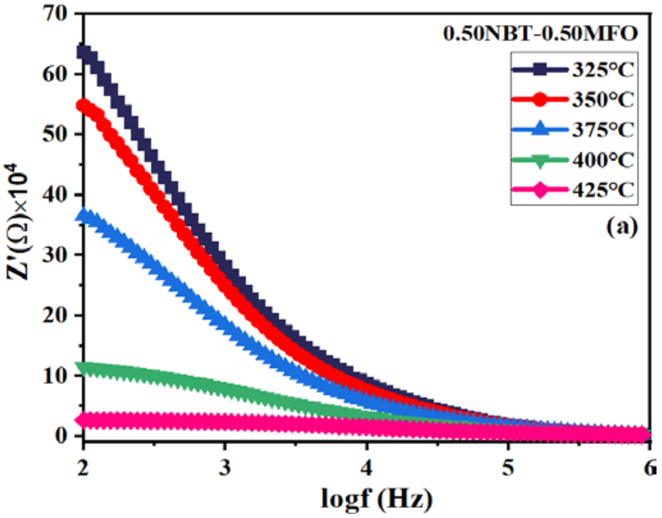

Figure 4(a). Frequency-dependent variation of the real impedance (Z′) for 0.50NBT-0.50MFO nanocomposite at different temperatures.

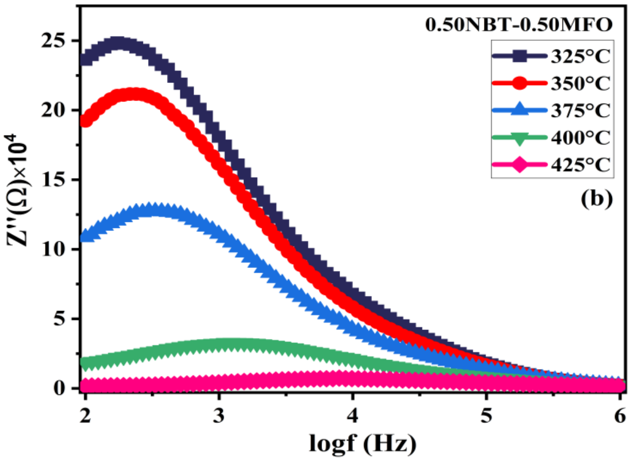

Figure 4(b). Frequency-dependent variation of imaginary impedance (Z″) for nanocomposite 0.50NBT-0.50MFO at different temperatures.

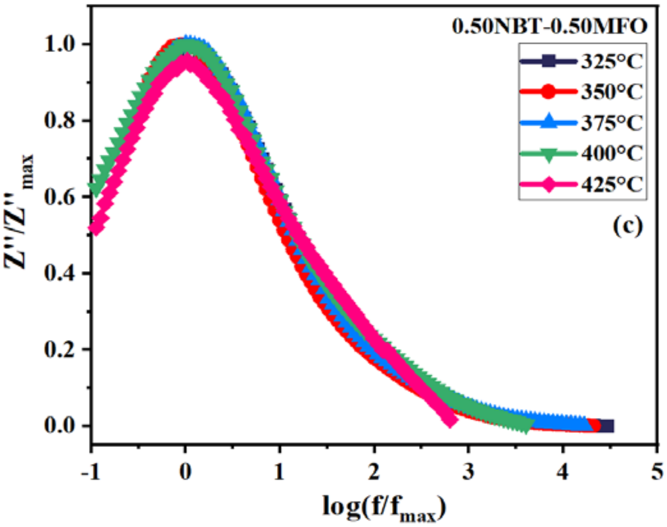

Figure 4(c). Frequency-dependent plot of the normalized imaginary impedance (Z''/Z''_{max}) for nanocomposite 0.50NBT-0.50MFO at different temperatures.

Modulus Analysis

Electrical Modulus investigation is an effective technique used to examine the electrical characteristics, particularly the conductivity & relaxation behavior, of materials such as ceramics. It provides insight into how materials respond to external electric fields at varying frequencies and temperatures. The electrical modulus, often denoted as M* is typically written as:

$$M^*=M'+iM'' \tag{5}$$

Where, $M'=$ □C_oZ' (the real part) represents the storage or energy conservation aspect of the material's response to the electric field and $M''=$ □C_oZ'' (the imaginary part) represents the dissipative or energy loss aspect, which is associated with resistive losses, such as those that occur due to the motion of charge carriers (electrons, ions, etc.) within the material.[29]

The real component of the modulus M′ is often inversely related to the ionic or electronic conductivity of the substance. As the frequency of the enforced electric field varies, the material's ability to conduct electricity can also change. Figure 5(a) illustrates the frequency-reliant variation of M′ for multiferroic 0.50NBT-0.50MFO nanocomposite at discrete temperatures. The comparatively modest value of M′ in the low-frequency range indicates the lack of electrode interactions and ionic polarization in the synthesized sample. As the frequency increases, M′ ascends, and this persistent dispersion with frequency implies a conduction mechanism governed by the short-range movement of charge carriers. This behavior can be ascribed to the lack of an attractive force, allowing charges to move in response to the applied external field. The rise in M′ with temperature signifies the thermal sensitivity of the relaxation process, while the shift of the dispersion zone to elevated frequencies suggests that charge carriers demonstrate long-range mobility.[30]

The imaginary part M″ helps analyze relaxation processes, which are phenomena where charge carriers (such as ions or electrons) take time to rearrange or reorient themselves in response to changes in the applied electric field. The relaxation behavior is important in understanding how the material's electrical response changes over time. For example, in ceramics, this can involve ionic diffusion or polarization relaxation.

Figure 5(b) depicts the behavior of M″ as a function of frequency at different temperatures for 0.50NBT-0.50MFO composition. As the frequency increases, M″ rises, reaching a maximal value, (M''_{max}) at a particular frequency. As the temperature increases, this peak migrates to higher frequencies, signifying a relaxation process influenced by temperature. The decrease in M″ beyond the peak indicates that the relaxation is predominantly driven by charge carriers hopping mechanism within the material. The variation in M''_{max} with temperature reflects changes in the sample's capacitance, where the peak magnitude is conversely proportional to capacitance. The frequency range before the peak is associated with charge carriers exhibiting extended mobility, whereas the range after the peak is linked to limited mobility, where carriers are confined within potential wells. The peak frequency signifies the shift from long-range mobility to short-range mobility of charge carriers, and this pattern is observed consistently in other samples as well. Figure 5(c) presents the scaling characteristics of normalized modulus isotherms, where the frequency axis is normalized by the maximum frequency (f_{max}) corresponding to the peak, and M″ is normalized by M''_{max}. The superposition of all the traces into a unified "master curve" across different temperatures demonstrates that the dynamic processes controlling conduction and relaxation are independent of one another. At reduced frequencies, minor deviations in the curves may be attributed to variations in the underlying relaxation processes.[12]

Figure 5(d) compares the imaginary components of impedance (Z″) and modulus (M″) as they vary with frequency. It is observed that Z″ and M″ exhibit distinct behaviors in terms of their symmetry and location of the peaks, indicating non-Debye relaxation dynamics and reinforcing the idea of a constant phase element within the circuit model. Specifically, the Z″ peaks exhibit asymmetry on the low-frequency end, while the M″ peak shows asymmetry on the high-frequency end. Throughout the full temperature spectrum, there is no overlap observed, suggesting that the samples display a combination of long-range conduction and confined relaxation processes. If the peaks in the merged graphs of Z″ and M″ align at an identical frequency, it suggests that the carriers of charge with long-range mobility contribute to the process of relaxation.[30]

Nyquist Plot

The impedance Nyquist plot (Cole–Cole plot) is presented in Figure 6(a) for all compositions at 400°C and in Figure 6(b) for 0.80NBT-0.20MFO composition at different temperature values. The plots reveal clearly defined, skewed semicircular arcs, with their centers positioned beneath the real Z′ axis, signifying that the samples exhibit non-Debye characteristics. This depression is often associated with systems that exhibit: distribution of relaxation times, non-ideal capacitive behavior, multiple relaxation processes, electrode surface homogeneity etc. In electrochemical systems, the ideal capacitor should form a perfect semicircular arc in the Nyquist plot. However, in real-world systems, imperfections such as surface roughness, non-uniform current distribution, or ionic conductivity issues often lead to deviations from this ideal behavior. The arc appears "depressed" because the capacitance behavior is not purely ideal but is influenced by factors such as constant phase elements (CPEs), which model the non-ideal capacitive behavior. CPEs are commonly employed to describe systems where the surface or interface is not perfectly smooth, and the electrochemical processes occur at multiple time scales or exhibit complex behaviors due to heterogeneities in the material or structure.[10]

These semicircles represent characteristic impedance behavior of the system and are indicative of relaxation phenomena, charge transfer, and energy storage mechanisms. In materials like ceramics, composites, or electrodes, there are various electrically active regions with different physical and electrochemical characteristics. These regions may include: grain structures, grain boundaries, and electrode interfaces. Each of these regions contribute independently to the overall impedance of the system, leading to multiple impedance responses, often observed as different semicircular arcs in the Nyquist plot. The grains

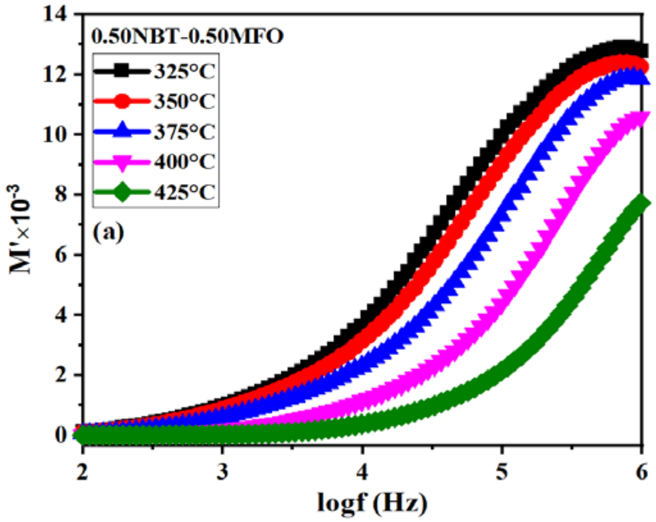

Figure 5(a). Frequency-dependence of real part of electric modulus (M′) for nanocomposite 0.50NBT-0.50MFO at different temperatures.

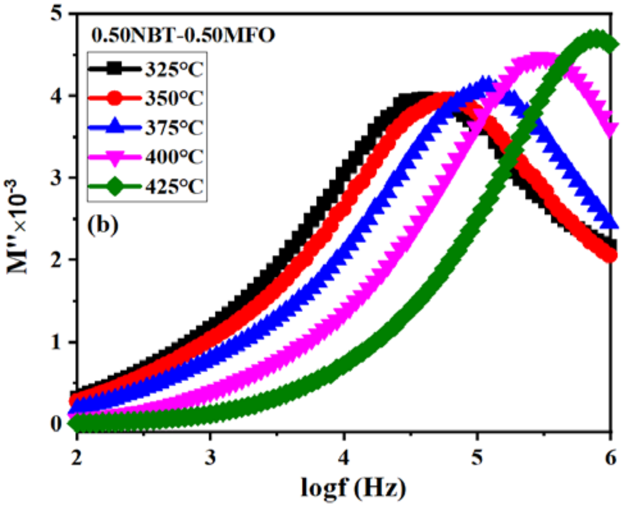

Figure 5(b). Frequency-dependence of imaginary part of electric modulus (M″) for nanocomposite 0.50NBT-0.50MFO at different temperatures.

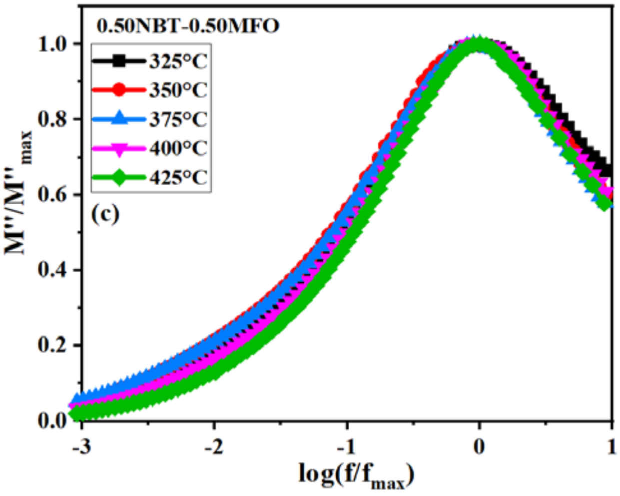

Figure 5(c). Electric modulus master curve at various temperatures for nanocomposite 0.50NBT-0.50MFO.

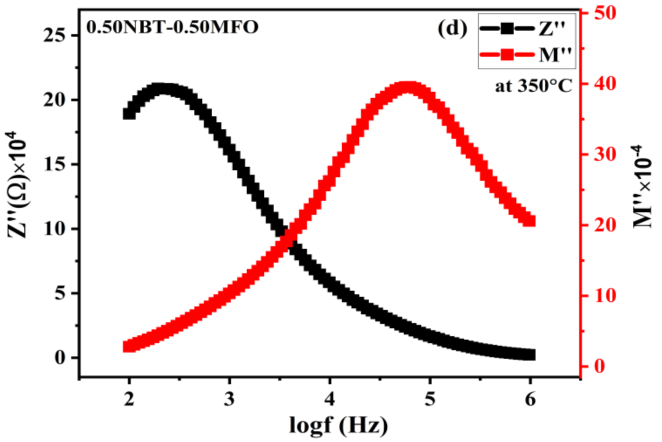

Figure 5(d). Frequency dependence of imaginary electric modulus (M″) and imaginary impedance (Z″) at 350°C for nanocomposite 0.50NBT-0.50MFO.

contribute to a higher-frequency arc, representing fast charge transfer processes occurring within the crystalline material. The grain boundaries, often associated with slower ion transport or higher resistivity, give rise to a lower-frequency arc. The electrode effects, such as the formation of an electric double layer and charge transfer resistance at the interface between the material and the electrolyte, also contribute a semicircle.[31] Thus, each of these electrically active domains can produce an individual arc, which, when combined, results in a composite Nyquist plot featuring multiple overlapping or distinct semicircles. High-frequency arcs typically correspond to capacitive effects or fast processes, whereas low-frequency arcs are generally related to diffusive or resistive processes[3]. To accurately interpret the impedance response and resolve the contributions of these various domains, equivalent circuit modeling is employed. The EC Lab V11.21 software is employed to correlate the experimental data with an equivalent circuit model through fitting.

An equivalent circuit generally includes a combination of resistors and capacitors, with the constant phase element (CPE) substituting the ideal capacitor to represent the system's non-Debye characteristics. The resistors in the circuit represent the bulk conductivity of the sample, reflecting its ability to conduct electrical current. Meanwhile, the capacitors in the model symbolize the space-charge distribution polarization occurring at the interfaces between the material and the electrodes, which arises due to charge accumulation in these regions. Figure 6(b) (inset) illustrates the corresponding circuit diagram derived from the impedance data of the synthesized samples. All the samples are represented by an equivalent circuit derived from the double-layer model, utilizing the formula provided below:

$$Z(f) = \frac{R_1R_2}{R_2+R_1(1+(i2\pi f)^{\alpha_1}Q_1R_2+(i2\pi f)^{\alpha_2}Q_2R_2)} \qquad (6)$$

Table 1 presents the fitted parameters, including resistances (R_1, R_2), constant phase elements (Q_1, Q_2), and relaxation time distribution (α_1, α_2), corresponding to both the grains and grain boundaries for all samples at 400°C. The α1 and α2 values range from 0.5 to 0.9, emphasizing the non-Debye relaxation and the classical Debye model as α approaches zero.[32] The impedance plots exhibit semi-circular curves, where the point of intersection on the real axis (Z′) corresponds to the materials' expected bulk resistance. As seen in figure 6(a), the incorporation of ferrite into the NBT phase leads to a reduction in the radius of the semicircular arc, indicating enhanced conductivity in the nanocomposites, with maximum conductivity in 0.50NBT-0.50MFO, although it remains lower than that of pure ferrite MFO. The pattern of conductivity shown by the plots is very relatable with the values of resistances R_1 and R_2 tabulated in table 1. As indicated in Table 1, it is evident that the grain boundaries exhibit higher values of resistance compared to the resistance of grains. The differing conductivity properties of the grains and their interfaces create a resistance zone, which contributes to a significantly elevated dielectric constant. As shown in Figure 6(b), as the temperature rises, the diameter of the semicircular arc decreases, and accompanied by a tilting of the arc closer to the real axis, indicating an improvement in the conductivity of 0.80NBT-0.20MFO nanocomposite sample. Similar behavior is observed in case of all other samples. This reduction in resistance with rising temperature suggests semiconductor-like behavior, consistent with a negative temperature coefficient of resistance (NTCR).[3]

Table 1. Grain and Grain boundary parameters of all samples at 400°C obtained from equivalent circuit fitting of Nyquist plots.

Sample	R_1 (MΩ)	R_2 (MΩ)	Q_1 (nF. $s^{(\alpha-1)}$)	Q_2 (nF. $s^{(\alpha-1)}$)	α_1	α_2
NBT	0.59	13.48	17.13	61.17	0.60	0.82
0.80NBT-0.20MFO	0.41	8.35	34.01	76.49	0.58	0.70
0.50NBT-0.50MFO	0.12	0.19	19.31	2.42	0.61	0.74
0.20NBT-0.80MFO	0.25	0.37	2.37	0.14	0.59	0.94
MFO	0.005	0.011	0.55	0.098	0.75	0.78

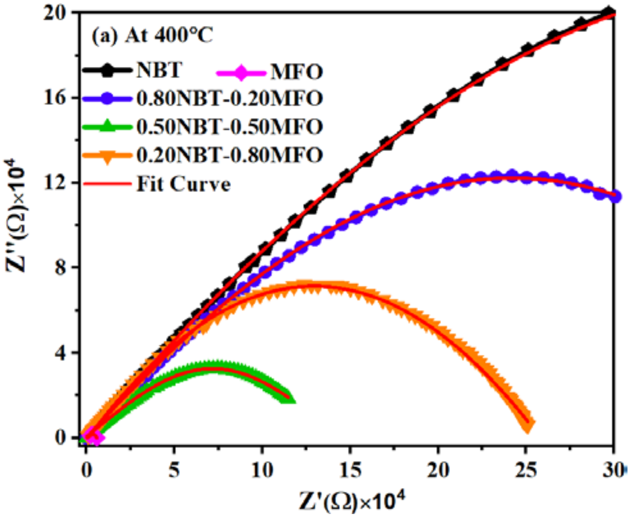

Figure 6(a). Nyquist plots of impedance (Z" vs. Z'), with fitted data derived from the equivalent circuit model, for all compositions at 400°C.

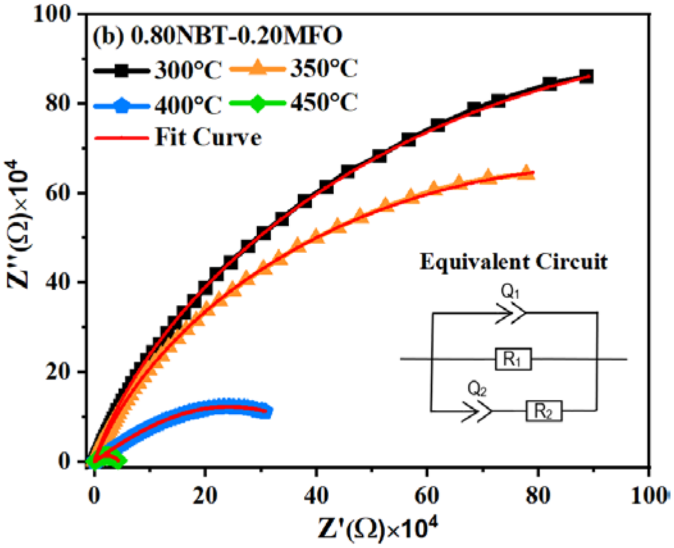

Figure 6(b). Nyquist plots of impedance (Z" vs. Z'), with fitted data derived from the shown equivalent circuit model, for nanocomposite 0.80NBT-0.20MFO at different temperatures.

CONCLUSION

The multiferroic nanocomposites with the general formula (1 - x) $Na_{0.5}Bi_{0.5}TiO_3$ - (x) $MgFe_2O_4$ (where x = 0, 0.2, 0.5, 0.8, 1.0) were effectively synthesized through the solid-state reaction technique, and their dielectric properties were comprehensively examined. Dielectric measurements conducted over varying frequencies and temperatures, revealed that both the dielectric permittivity (ε′) and dielectric loss (tanδ) diminished in higher frequency domain, while increasing with temperature, displaying a dispersive behavior in the low-frequency and elevated temperature regions. The frequency-dependent behavior of capacitance and dielectric constant in the wet state underscored the promising potential of these compositions for electrical energy generation in hydroelectric cell applications. Dielectric dispersion in these nanocomposite-based cells fosters the formation of a double capacitive layer, while the elevated capacitance observed in the wet state suggests a significant surface or interfacial charge, arising from enhanced chemidissociation within the hydroelectric cells. The convergence of the normalized impedance and modulus curves, onto a unified master curve firmly substantiated the presence of a relaxation phenomenon in the developed system, suggesting that the system exhibits a singular relaxation process across all temperature ranges. The non-Debye behavior was validated through a meticulous comparison of the impedance and electric modulus plots. The Nyquist impedance diagrams revealed skewed semicircular arcs, and the observed contraction of the arc radii with rising temperature further affirmed the semiconducting characteristics inherent in the synthesized system. The distortion of arcs pointed to a non-Debye relaxation process, which can be ascribed to the imperfections present in the samples, suggesting a deviation from ideal relaxation behavior. These dilectric materials with high dielectric constants at low frequencies and high temperatures are hence integral to applications in electronics, communications, energy storage, and sensor technologies, where reliable performance in extreme conditions is essential.

ACKNOWLEDGMENTS

Monika Dhall would like to thank DCRUST, Murthal for providing financial support under URS. Authors are thankful to DST Delhi (India) for their experimental support through FIST research grant (Sanction order No. and Date: SR/FST/PS-1/2018/32).

CONFLICT OF INTEREST STATEMENT

The authors declare that they have no known competing financial interests or personal relationships that could have appeared to influence the work reported in this paper.

REFERENCES AND NOTES

1. S. Sahoo, A. Yadav, K.P. Andryushin, P.K. Mahapatra, R.N.P. Choudhary. Structural transformation, dielectric and multiferroic properties of (Gd1-xBax)(Fe1-xTix)O3 ceramics by tuning composition. *Ceram. Int.* **2023**, 49 (1).
2. R.S. Devan, B.K. Chougule. Magnetic properties and dielectric behavior in ferrite/ferroelectric particulate composites. *Phys. B Condens. Matter* **2007**, 393 (1–2), 161–166.
3. S. Dagar, A. Hooda, S. Khasa, M. Malik. Structural refinement, investigation of dielectric and magnetic properties of NBT doped BaFe12O19 novel composite system. *J. Alloys Compd.* **2020**, 826, 154214.
4. S. Dagar, A. Hooda, S. Khasa, M. Malik. Investigations of structural, enhanced dielectric and magnetic properties of NBT doped ferrite system. *Mater. Chem. Phys.* **2020**, 249 (January), 123214.
5. S.N. Babu, K. Srinivas, T. Bhimasankaram. Studies on lead-free multiferroic magnetoelectric composites. *J. Magn. Magn. Mater.* **2009**, 321 (22), 3764–3770.
6. K. Praveena, K.B.R. Varma. Enhanced electric field tunable magnetic properties of lead-free Na0.5Bi0.5TiO3–MnFe2O4 multiferroic composites. *J. Mater. Sci. Mater. Electron.* **2014**, 25 (12), 5403–5409.
7. J. Shah, R.K. Kotnala, B. Singh, H. Kishan. Microstructure-dependent humidity sensitivity of porous MgFe2O4-CeO2 ceramic. *Sensors Actuators, B Chem.* **2007**, 128 (1), 306–311.
8. S. Thakur, K. Parmar, S. Sharma, N.S. Negi. Structural, Magnetic, and Electrical Properties of (1-x) Na0.5Bi0.5TiO3 –(x) NiFe2O4(x = 0.1, 0.3, 0.5, 0.7, and 0.9) Multiferroic Particulate Composite. *J. Supercond. Nov. Magn.* **2021**, 34 (2), 489–495.
9. S. Dagar, A. Hooda, S. Khasa, M. Malik. Rietveld refinement, dielectric and magnetic properties of NBT-Spinel ferrite composites. *J. Alloys Compd.* **2019**, 806, 737–752.
10. M. Dhall, S. Khasa, A. Hooda, J. Shah, R.K. Kotnala. Nanocomposite NBT-MFO for eco-friendly power generation: Self sustainable hydroelectric cell. *Ceram. Int.* **2024**, 50 (10), 17570–17592.
11. R. Nongjai, S. Khan, K. Asokan, H. Ahmed, I. Khan. Magnetic and electrical properties of in doped cobalt ferrite nanoparticles. *J. Appl. Phys.* **2012**, 112 (8).
12. P. Dahiya, A. Hooda. Efficiently high energy storage density in Ba2+ ion modified K0·5Na0·5NbO3 (KNN) ferroelectric ceramics for super capacitors. *Mater. Chem. Phys.* **2024**, 323 (June).
13. S. Qu, G. Wu, J. Fang, et al. Dielectric and Magnetic Loss Behavior of Nanooxides; Elsevier Inc., **2017**; Vol. 2.
14. C. Li, G. Chen, X. Qiu, Q. Lou, X. Gao. A direct proof for Maxwell-Wagner effect of heterogeneous interface. *AIP Adv.* **2021**, 11 (6), 1–8.
15. C.G. Koops. On the dispersion of resistivity and dielectric constant of some semiconductors at audiofrequencies. *Phys. Rev.* **1951**, 83 (1), 121–124.
16. M.F.A. Bin Zolkepli, Z. Zainuddin. Structural, magnetic and electrical properties of barium titanate and magnesium ferrite composites. *Sains Malaysiana* **2017**, 46 (6), 967–973.
17. V.R. Mudinepalli, F. Leng, M.P. Reddy, W.C. Lin, B.S. Murty. Structural, dielectric and ferroelectric properties of lead-free Na0.5Bi0.5TiO3 ceramics prepared by spark plasma sintering technique. *Indian J. Phys.* **2016**, 90 (2), 131–138.
18. B.V.B. Saradhi, K. Srinivas, T. Bhimasankaram. ELECTRICAL PROPERTIES OF (Na1/2Bi1/2)1−xCaxTiO3 CERAMICS. **2002**, 16 (27), 4175–4187.
19. B.K. Barick, K.K. Mishra, A.K. Arora, R.N.P. Choudhary, D.K. Pradhan. Impedance and Raman spectroscopic studies of (Na0.5Bi 0.5)TiO3. *J. Phys. D. Appl. Phys.* **2011**, 44 (35).
20. N. Adhlakha, K.L. Yadav. Study of structural, dielectric and magnetic behaviour of Ni 0.75Zn0.25Fe 2O4-Ba(Ti 0.85Zr 0.15) O 3 composites. *Smart Mater. Struct.* **2012**, 21 (11).
21. B. Bhushan. Tribology and Mechanics of Magnetic Storage Systems., 2nd ed.; Springer New York, NY, **1996**.
22. Z. Yu, C. Ang. Maxwell-Wagner polarization in ceramic composites BaTiO3-(Ni0.3Zn0.7)Fe2.1O 4. *J. Appl. Phys.* **2002**, 91 (2), 794–797.
23. K. Sarkar, S. Mukherjee. Synthesis, Characterization and Property Evaluation of Single Phase MgNb 2 O 6 by Chemical route. *J. Aust. Ceram. Soc.* **2016**, 52 (2), 32–40.
24. J.C.R. Araújo, S. Araujo-Barbosa, A.L.R. Souza, et al. Tuning structural, magnetic, electrical, and dielectric properties of MgFe2O4 synthesized by sol-gel followed by heat treatment. *J. Phys. Chem. Solids* **2021**, 154 (November 2020).
25. R. Gupta, J. Shah, R. Singh, R.K. Kotnala. Nonphotocatalytic Water Splitting Process to Generate Green Electricity in Alkali Doped Zinc Oxide Based Hydroelectric Cell. *Energy and Fuels* **2021**, 35 (11), 9714–9726.
26. R. Qindeel, N.H. Alonizan. Structural, dielectric and magnetic properties of cobalt based spinel ferrites. *Curr. Appl. Phys.* **2018**, 18 (5), 519–525.
27. D.K. Mahato, A. Dutta, T.P. Sinha. Impedance spectroscopy analysis of double perovskite Ho 2NiTiO6. *J. Mater. Sci.* **2010**, 45 (24), 6757–6762.
28. W. Shi, Y. Feng, T. Lu, et al. Photoluminescence and impedance properties of rare-earth doped (K0.5Na0.5)NbO3 lead-free ceramics. *J. Mater. Sci. Mater. Electron.* **2019**, 30 (1), 9–16.
29. S. Dagar, A. Hooda, S. Khasa. Dielectric properties, complex impedance analysis and electrical properties of novel particulate composites of NBT-SrFe12O19. *J. Mater. Sci. Mater. Electron.* **2020**, 31 (14), 11609–11617.
30. R. Das, R.N.P. Choudhary. Dielectric relaxation and magneto-electric characteristics of lead-free double perovskite: Sm2NiMnO6. *J. Adv. Ceram.* **2019**, 8 (2), 174–185.
31. V. Kumar, R.K. Singh, A. Manash, et al. Structural, optical and electrical behaviour of sodium-substituted magnesium nanoferrite for hydroelectric cell applications. *Appl. Nanosci.* **2022**.
32. Manjusha, M. Rawat, K.L. Yadav. Structural, Dielectric, Ferroelectric and Magnetic Properties of (x) CoFe2O4-(1-x) BaTiO3 Composite. *IEEE Trans. Dielectr. Electr. Insul.* **2015**, 22 (3), 1462–1469.